



Original Contribution

SPATIAL COMPOUNDING IN ULTRASONIC IMAGING USING AN ARTICULATED SCAN ARM

A. HERNANDEZ,[†] O. BASSET,[†] P. CHIROSSEL[‡] and G. GIMENEZ[†]

[†]CREATIS URA CNRS 1216, INSA Lyon, France; and

[‡]Hôpital Cardio-Vasculaire et Pneumologique Louis Pradel, service de radiologie, Bron, France

(Received 26 January 1995; in final form 28 July 1995)

Abstract—A spatial compounding system has been designed to improve the quality of B-mode echographic images. It consists of constructing an improved image from the combination of several different images of the same cross-sectional plane. The “final” image is constructed by the registration and the superposition of the “original” images. For this, the relative position in the space of the original images has to be known. The use of a localization articulated arm, on which the ultrasonic probe is fixed, makes this possible. The main advantages of the technique are, on one hand, the elimination of the acoustic shadows following a strong reflector structure and, on the other hand, the reduction of the speckle generated in echographic images. The method of reconstruction has been validated on agar gel phantoms and provides good accuracy. *In vivo* experiments on human beings have also been performed. Acoustic shadows caused by bones in cross-sectional images of the thigh and the arm are eliminated. All the contours of the femur and humerus can be observed in the final images. The reduction of speckle is shown in kidney images and the signal-to-noise ratio improvement is quantified as a function of the number of images involved in the reconstruction.

Key Words: Spatial compounding, Articulated scan arm, B-scan echography, Acoustic shadow suppression, Acoustic speckle reduction, Image reconstruction, Registration.

INTRODUCTION

Some years ago, an articulated arm was used to localize a single transducer element in a manual contact B-scan imaging system. Such a system has been described by Wells (1977). Since then this system has been abandoned and replaced by mechanical and electronic probes which have allowed for the development of real-time systems. However, the localization arm is still used in some three-dimensional imaging applications (Hottier and Collet Billon 1990; Nikravesh et al. 1984).

In this study, another useful feature of the scan arm is explored: spatial compounding. This technique consists of superposing several B-scan images acquired in the same plane but with different orientations of the probe. To register these images, it is necessary to know the position of the transducer probe during the acquisition step. This position is calculated from the information returned by a coordinate measurement system on which the probe is fixed. Generally, the localization systems allow just 1 degree of freedom to the probe, like a rotation or translation. Thus, the position of the

probe in a spatial coordinate system is easily calculated and these systems can be motorized. But with such simple movements the probe cannot stay permanently in contact with the investigated object and a liquid coupling is necessary. For instance, the object can be immersed in a water tank. This is constraining, especially for medical examinations in which patient and operator comfort must be taken into consideration. The articulated arm with its several degrees of freedom can be a useful alternative to a water-path system. It permits spatial localization of the transducer probe, which is fixed at its end and, in addition, can be placed in direct contact with the skin of the patient.

The acoustic shadows and the speckle are specific phenomena to ultrasonic images which reduce the legibility of images. The spatial compounding technique is a way of limiting their effect.

When an ultrasonic beam investigates a medium in which a structure has an impedance very different from that of the surrounding tissue, the interface medium/structure reflects very greatly the incident ultrasonic energy. This strong reflector usually generates, on B-mode echographic images, a shadow cone followed by a white line. The shadow cone corresponds

Address correspondence to: Dr. Ange Hernandez, CREATIS URA 1216, INSA Lyon, 69621 Villeurbanne Cedex, France.

to the area that the ultrasounds cannot explore, and the white line indicates the reflecting interface. In some cases, the acoustic shadow can be an indication of a pathology. For example, it allows the identification of stones in the gall bladder or kidney (Diamant et al. 1986). In other cases, shadows are a nuisance because a part of the information is missing in the image behind the strong reflector. The most frequent acoustic shadows are generated by bones, which are strong reflectors in comparison with soft tissues. The information related to the shadow zone is only accessible by an exploration of the medium with a different incidence.

As a noninvasive and nonionizing radiative technique of investigation, B-scan echography is a common way of monitoring skeletal growth of the lower limbs in infants. Primarily the hip is investigated, especially for the detection of luxations and dysplasias (Graf 1984). Because of the shadow area generated by this bone structure, the operator must mentally integrate several partial and complementary views obtained around this structure to estimate its geometry.

Acoustic tomography (Dines and Goss 1987; Greenleaf and Bahn 1981; Jago and Whittingham 1992) is a technique which can be used to avoid shadows. It was implemented by Sehgal et al. (1988) to construct cross-sectional images of turkey and dog limbs. These reconstructed images show bone contours and the surrounding soft tissues without shadows. Ultrasonic tomography provides relatively high quality images. Nevertheless, computation of reconstruction uses complex and time-consuming algorithms. Moreover, a particular setup is necessary to make the transducer describe a circular movement around the structure which is immersed in a water tank.

Compared to ultrasonic tomography, spatial compounding has a negligible calculation time. It would be interesting to apply this technique to acoustic shadow suppression generated by bones.

The presence of large quantities of scattering elements in biological tissues on echographic images generates a granular texture called *speckle* (Burckhardt 1978). The scatterers within an elementary resolution cell emit wavelets that interfere with each other. Interferences which are mainly constructive give a high-amplitude echo on the image; those which are mainly destructive give a low-amplitude echo. Because of the speckle, the information in the image corresponding to the large structure (specular reflexion) is blurred and the image has low contrast. Speckle reduction is a field of research which has been explored largely to improve the image quality and to increase the signal-to-noise ratio. Several studies have shown the virtual elimination of speckle by using the technique of spatial compounding (Friedrich et al. 1982; Jago and Whitting-

ham 1992; Trahey et al. 1986; Shattuck and von Ramm 1982). To our knowledge, however, none of these studies uses an articulated arm with a real-time scanning probe specifically to reduce speckle.

The B-scan arm, the method of image reconstruction and the validation of this method are described in the first part of this article. Then the results are presented for *in vivo* applications in the second part.

METHODS

Data acquisition

The acquisition of the spatial coordinates of the images is done with the articulated scan arm represented in Fig. 1. It is composed of several segments linked to each other by six articulations. The first segment is fixed on a support which is immobile in the reference laboratory. The other extremity of the articulated arm, on which the transducer probe is fixed, can move within a large volume of interest because of the 6 degrees of freedom given by the articulations. The knowledge of the different segment lengths and of the angular values transmitted from each articulation allow us to calculate the echographic probe position in a

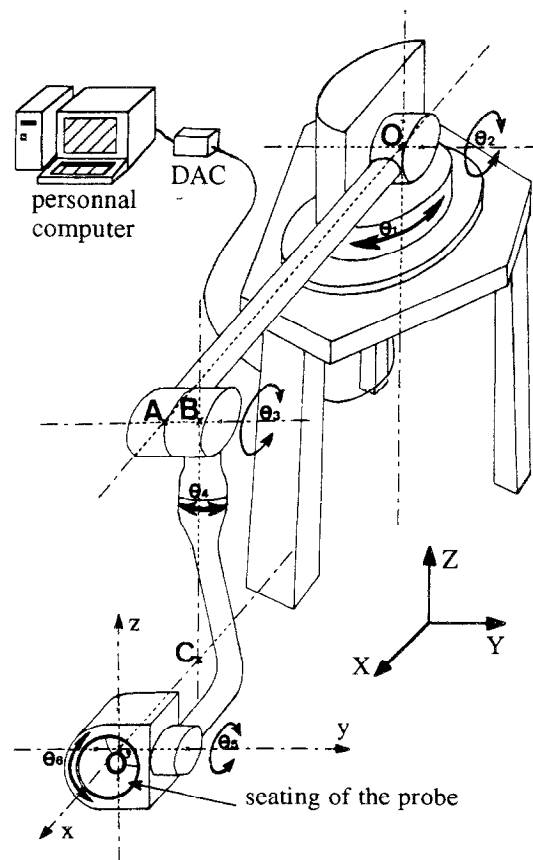


Fig. 1. Schematic representation of the articulated scan arm.

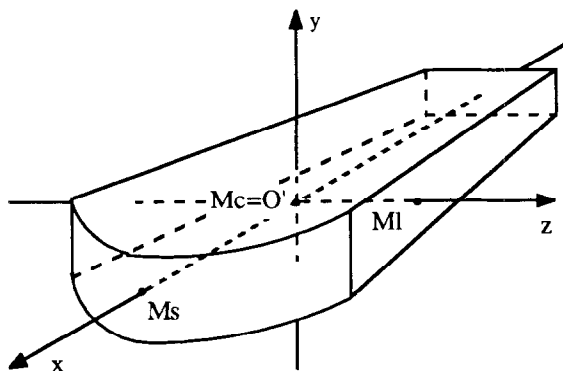


Fig. 2. Position of the three points: Ms, Mc and Ml with regard to the phased-array transducer in the coordinate system (O' , x , y , z).

coordinate system relative to the support, after six successive coordinate system changes. The angular values are given by a potentiometer placed in each articulation. This returns an electrical voltage proportional to the rotation angle of the articulation. The electrical signals provided by the six articulations are converted into digital signals with a digital-to-analog converter (DAC). Then they feed a computer (PC 386, 33 MHz) via an acquisition card (Nautil Logic-40). The localization of the probe can be calculated and, consequently, so can the spatial position of the corresponding image.

To specify the image plane and the localization of the image in this plane, three particular points relative to the probe are defined. These points (Ms, Mc and Ml [s for source, c for center and l for lateral]) are placed, as shown in Fig. 2, in the coordinate system (O' , x , y , z) of the probe. After being calculated in the coordinate system (O , X , Y , Z) of the laboratory, the point coordinates give us the equation of the ultrasonic beam exploration plane. The vector, \overline{McMs} , defines the image orientation. Ms is a point corresponding to the extremity of the probe and is also a specific point easily identifiable in the sectorial images as shown in Fig. 3. The position of the echographic image in the image plane is known because of this point. The software developed with the scan arm allows us to calculate the coordinates of Ms, Mc and Ml, and to store them with a reference to the corresponding image.

For the echographic image acquisition, an image is frozen on the scan screen simultaneously with the corresponding coordinate acquisition of the probe. The image is then digitized and stored in the PC. The ultrasonic scanner is a Radius (General Electric), equipped with two sectorial phased arrays of 3.5 MHz (HRA) and 7.5 MHz (MRA). The images are digitized with a Matrox PIP 1024 card, in 512×512 pixels, with

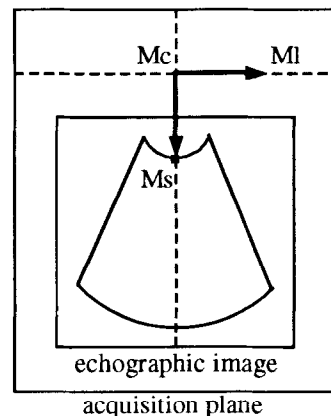


Fig. 3. Position of the three points: Ms, Mc, and Ml on an echographic image.

256 grey levels. The acquisition setup of the images and their coordinates is presented in Fig. 4.

The various images used for spatial compounding must be acquired in the same cross-sectional plane. The rotation planes of the last three articulations of the scan arm (the nearest to the probe) are not parallel, so there is no mechanical constraint which maintains the probe in the same scanning plane. To resolve this difficulty, a reference plane corresponding to the first image plane is defined, and for the acquisition of the other images the software displays information to help the operator keep the probe in the same plane. In fact, the reference plane is a "slice" and an image is considered as belonging to it if the three points, Mc, Ml and Ms, are included in this slice. Obviously, the thinner

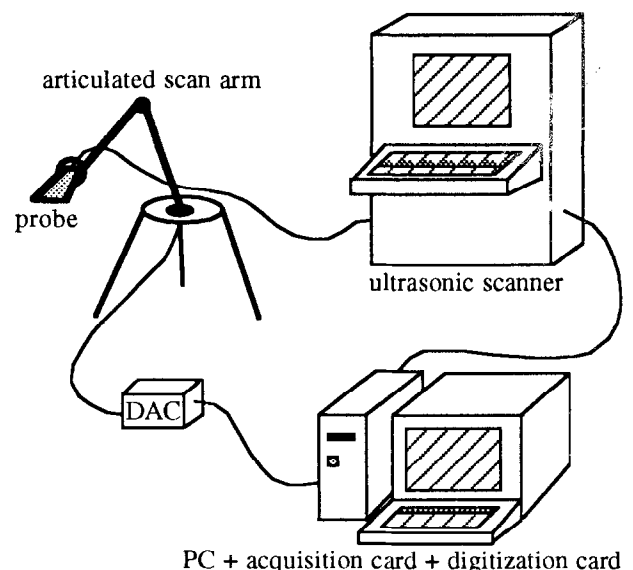


Fig. 4. Connection of the different equipment allowing the acquisition of images and their spatial coordinates.

the slice, the more accurate the reconstruction, but the more difficult the operator manipulation.

Image reconstruction phase

The first step of image reconstruction is the registration of the images obtained under different angles of view, in the same cross-sectional plane, during the acquisition phase. For clarity, the registration technique is described from only two original images: image 1 and image 2. Image 1 stays fixed in the screen plane. Image 2 undergoes a rotation and a translation to be registered with respect to image 1. The rotation center is the pixel which corresponds to point Ms in image 2. The rotation angle and the translation parame-

ters are calculated from the coordinates of each image stored in the computer.

Some holes appear in image 2 after rotation. They are removed by an interpolation filter applied to the whole image.

The fusion of the registered images is the second step of the reconstruction phase. Two methods of fusion have been implemented. The first method of fusion is the maximum value algorithm. Each pixel of the reconstructed image receives the highest grey level of the corresponding pixels of the N -registered images. This method is of interest for acoustic shadowing suppression. It allows the visualization of strong reflector contours with the acquisition of few images. The

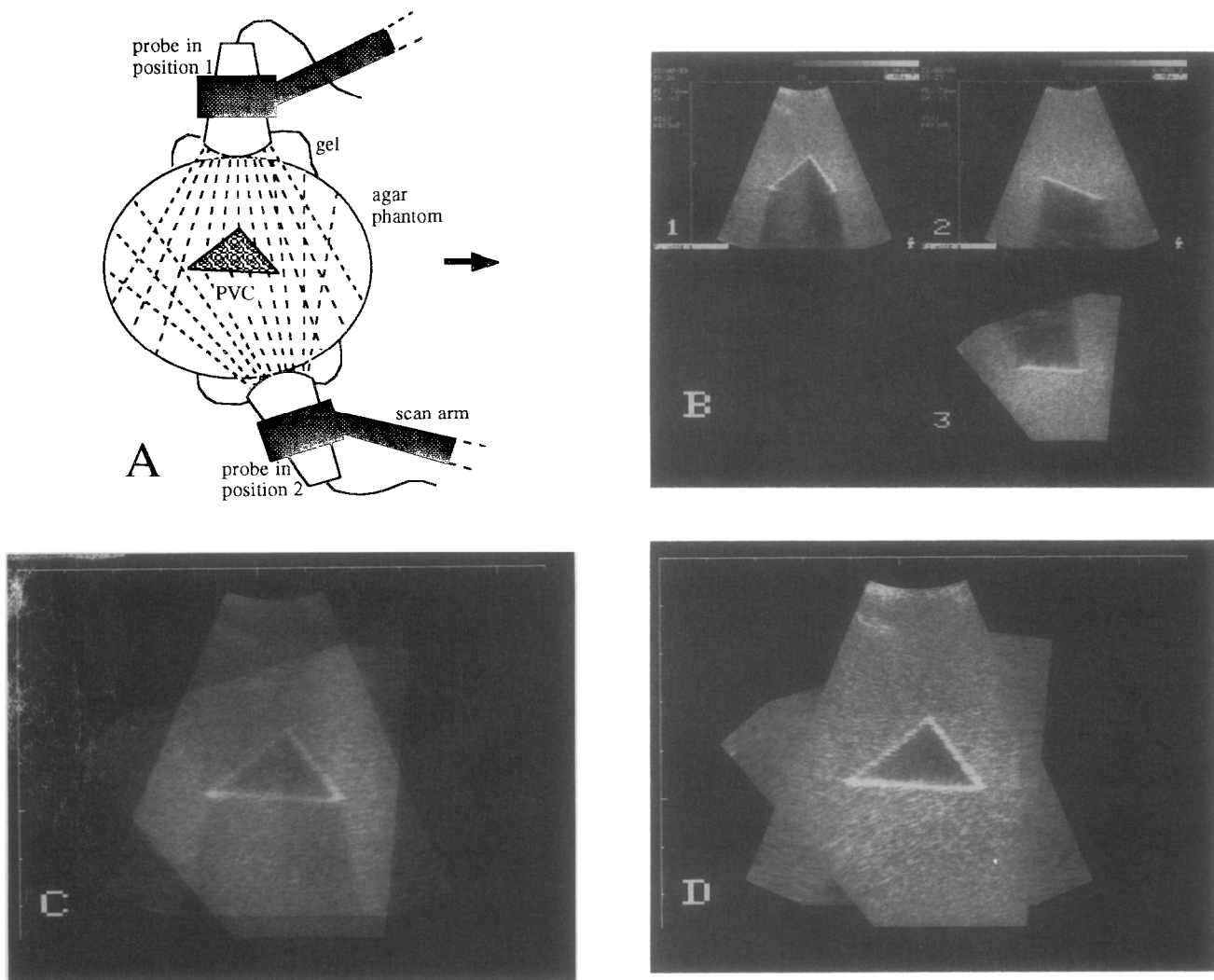


Fig. 5. Acquisition, registration and fusion on phantom images to validate the reconstruction method for acoustic shadowing suppression. The diagram (A) indicates the positions of the probe, around an agar phantom, with a hyperechoic structure during the acquisition phase. Image (B1) is acquired by the probe in position 1 and image (B2) in position 2. Image (B3) corresponds to image (B2) after the registration. The fusion of image (B1) with image (B3) gives image (C) using the average value algorithm, and image (D) using the maximum value algorithm. The vertical and horizontal axes are graduated each centimeter.

shadow regions are eliminated because they have low grey levels, while the strong reflector contours are preserved because they have high grey levels. On the other hand, this method suffers from a serious sensitivity to noise problem, as the noise increases with the number of images.

The second method of fusion is the average value algorithm. The reconstructed image is the average, pixel-to-pixel, of the N -registered images. This method is used for speckle reduction. In contrast to the former method, the greater the number of images, the more the noise is attenuated. This method, applied to the acoustic shadowing reduction, leads to a decrease in the contrast on the strong reflector contours.

Validation of the reconstruction method using phantoms

Phantoms made with agar gel were used. The ultrasonic properties (velocity and impedance) in agar at a temperature of 37°C are approximately equal to those of soft tissues. The B-scan imaging system uses the mean velocity of ultrasonic propagation in tissues (1540 m/s) for the generation of images. To avoid the geometrical distortions of the images, the temperature of agar phantoms was kept at 37°C.

The method of reconstruction was validated for the suppression of acoustic shadows on an agar gel phantom which contains a strong PVC reflector with a triangular section (Fig. 5a). From images 1 and 2 of Fig. 5b, cross-sections of this phantom were reconstructed with attenuated shadows in Fig. 5c (average value algorithm) and without shadows in Fig. 5d (maximum value algorithm). The shape and dimensions of the triangle in the reconstructed images were in accordance with those measured on the PVC structure. Moreover, the continuity of contours was preserved.

The reconstruction method was also validated on another agar phantom for speckle reduction. The latter consisted of a cylinder of agar mixed with talc, 2.3 cm in diameter, included in a larger cylinder made entirely of agar. The talc was added to modify slightly the acoustic properties in the small diameter cylinder. Sixteen cross-sectional images were acquired around this phantom with a slightly different angle of view. One of these images is presented in Fig. 6a. These images were then registered and averaged. The reconstructed image is presented in Fig. 6b. The visual observation of this figure shows an obvious reduction of speckle. The two regions, the disk and the surrounding medium, show a more homogeneous texture and the artefacts are eliminated. Nevertheless, the contours remain blurred. The spatial compounding does not improve the accuracy of structure contours. This can be explained in several ways. First, the error of the localization device

leads to registration errors of the various images. Then, as the velocity of ultrasound is not homogeneous in the different structures, the reconstructed images present a small distortion of the shape of the investigated structure. Therefore, these images cannot be registered perfectly. Finally, when the ultrasonic beam encounters a contour under an oblique incidence, the contour is constructed with poor resolution corresponding to the lateral impulse response of the transducer.

A quantitative estimation of the signal-to-noise ratio improvement will be presented in the following section.

Accuracy

The quality of a reconstructed image can be assessed from various criteria: the contour continuity of the structures; the accuracy of reconstructed structure size; resolution; contrast; and so forth. All of these points depend on the accuracy of the matching of the original images. The main source of matching errors is due to the localization accuracy of the articulated arm.

The localization error of the articulated scan arm was estimated. For this, a stylus was fixed to the end of the arm. Its tip was positioned at a point of space where the coordinates were known exactly. The software computes the coordinates of this point. Then the error for one configuration of the articulated localization system and for one point of the space could be calculated. This error corresponds to the distance between the actual point and the calculated point. This manipulation was repeated for different articulation configurations of the scan arm with the same point and then for different points of the space. The average of the magnitude of all the error vectors is 0.7 mm and the maximum recorded error is 1.2 mm. These errors are quite acceptable because they are in the same range order as the axial and lateral resolutions of the echographic images.

RESULTS

Acoustic shadowing suppression

Cross-sectional images were realized, *in vivo*, on the arm (Fig. 7a) and the thigh (Fig. 7d) of a human. During acquisition of these images, a support was used to hold the arm or the thigh immobile to avoid errors due to movement. An echographic probe of 3.5 MHz was used for data acquisition on the femur and the other one of 7.5 MHz for data acquisition on the humerus. A standard gel was used as a coupling medium between the probe and the patient's skin. Reconstruction images (Fig. 7b and c) allow the visualization of humerus contours, respectively, by the above-mentioned maximum and average value algorithms. Recon-

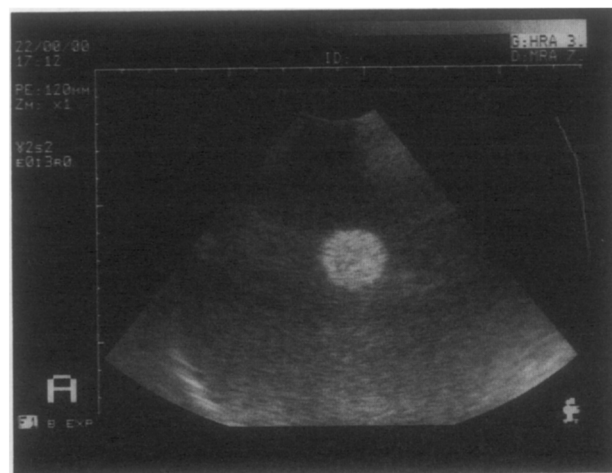


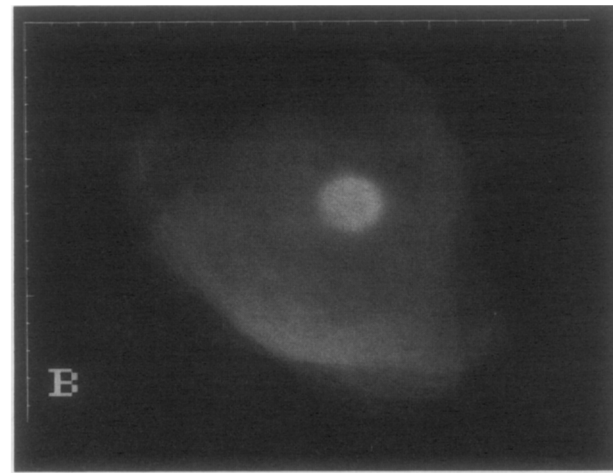
Fig. 6. Validation of the reconstruction method for acoustic speckle reduction. Image (B) is reconstructed from the registration and the averaging of 16 independent images, acquired on the same plane of an agar phantom. Image (A) shows one of these images.

structed images (Fig. 7e and f) show the femur contours. On these cross-sectional images of long bones, the acoustic shadows are suppressed and the bone contours are clearly visible. The bone dimensions seem to be correct and the contour continuity is verified. The reconstructed images only show three fourths of the humerus and femur contours. In fact, the articulated scan arm used has limited ranges of rotation. Therefore, in a given plane, the rotation of the probe cannot be more than 180°.

Acoustic speckle reduction

In vivo speckle reduction was realized from cross-sectional images of a normal subject's abdomen. These images show a partial view of the kidney and liver of this patient. Figure 8a presents one of the 11 images acquired. The original images were all recorded at a same stage of the breathing activity to limit abdominal organ movements and subsequent reconstruction errors. Figure 8b shows the reconstructed image, after the registration and the average of only 6 of the 11 images which were acquired. In fact, $N = 6$ images seems to be, in this case, the best compromise between speckle reduction and the preservation of tissue details.

The necessary condition to reduce speckle efficiently by spatial compounding is the decorrelation of the ultrasonic signals of each original image. To achieve this, the original images must be acquired with different incidences. Burckhardt (1978) calculated theoretically that the signal amplitude of two adjoining exploration lines is "almost" decorrelated if the transducer is moved by half its width. In our study, to decorrelate the images obtained, the echographic probe underwent a rotation of an angle of nearly 4° and a



translation of nearly 5 mm between each successive acquisition.

The echo-amplitude histogram of a B-mode speckle image generated from a homogeneous scattering medium has a Rayleigh probability density function when the number of scatterers per resolution cell is large. It can be assumed that this condition has been respected in our experiments. The ratio of the mean grey level (μ) to the standard deviation (σ) is commonly called the signal-to-noise ratio at a point (SNR), and its inverse is the speckle contrast. In the case of a Rayleigh distribution, the SNR is constant and is equal to 1.91. Generally, in ultrasonic scanners, the ultrasonic amplitude data undergo a logarithmic compression. The echo-amplitude distribution of the speckle in a region of interest then has a Gaussian shape (Crawford et al. 1993). SNR in such an image increases approximately by a factor of four with respect to a noncompressed image (Thijssen et al. 1988).

The higher the number of averaged images, the more spatial compounding reduces speckle. In fact, the average of n -matched images with uncorrelated signals theoretically increased the SNR by a factor of \sqrt{n} . This point has been verified in this study by the representation of the mean SNR as a function of n . The method of SNR estimation is described above.

In a given work window, each registered image has not entirely the same SNR. According to how n of these images are chosen among the total image number N , the resultant image does not present the same SNR. There are C_N^n ways to combine n images selected from N , and then there are $k \in [1 \cdots C_N^n]$ different final images. The SNR is first calculated for each k final image by using the following expressions:

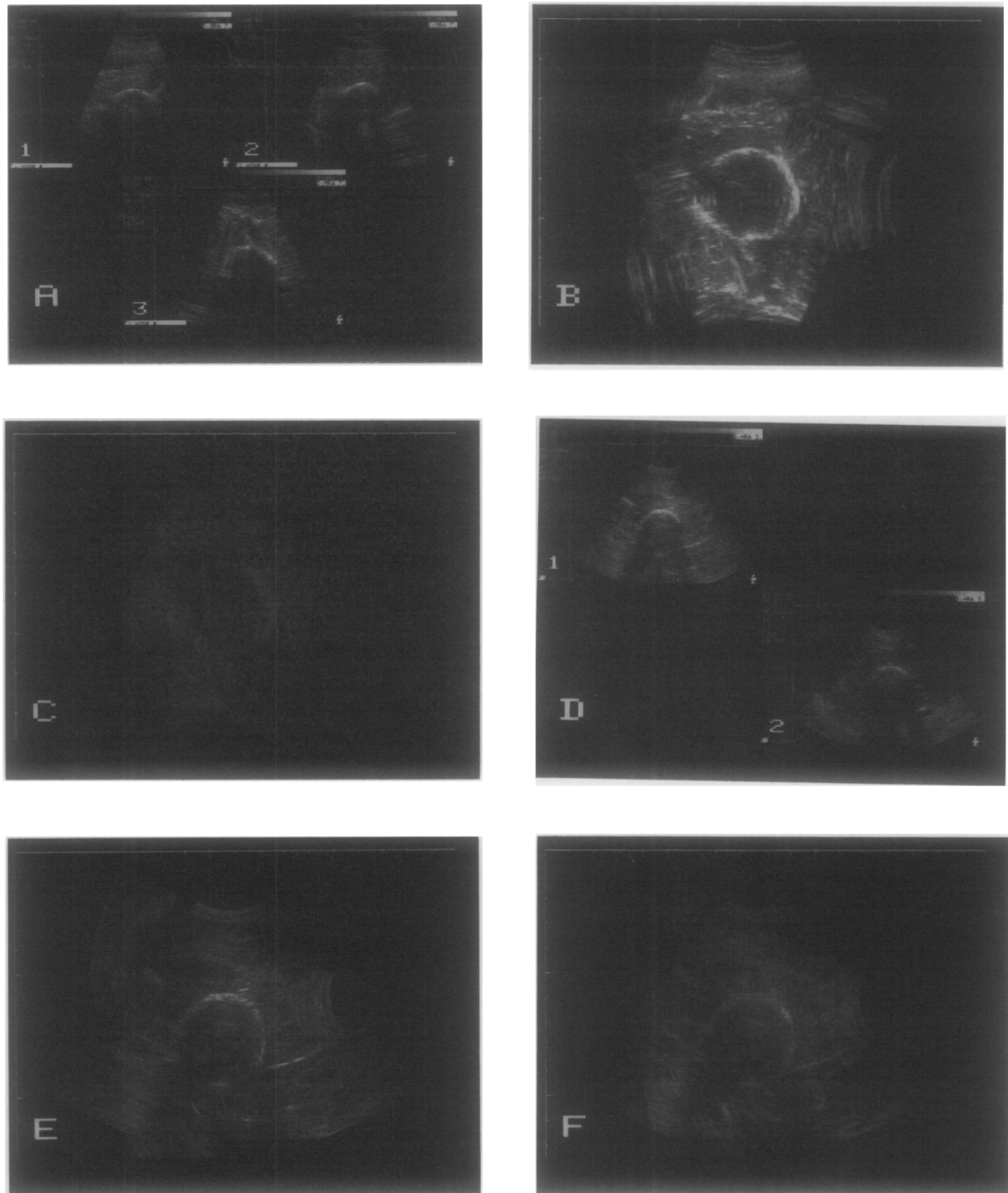


Fig. 7. Reconstruction of cross-section long bone images: (A) cross-section images acquired in a same plane around a patient's arm; (B) and (C) reconstruction of a cross-section image of this arm by the maximum and the average value algorithms, respectively; (D) cross-section images acquired in a same plane around a patient's thigh; and (E) and (F) reconstruction of a cross-section image of this thigh by the maximum and the average value algorithms, respectively.

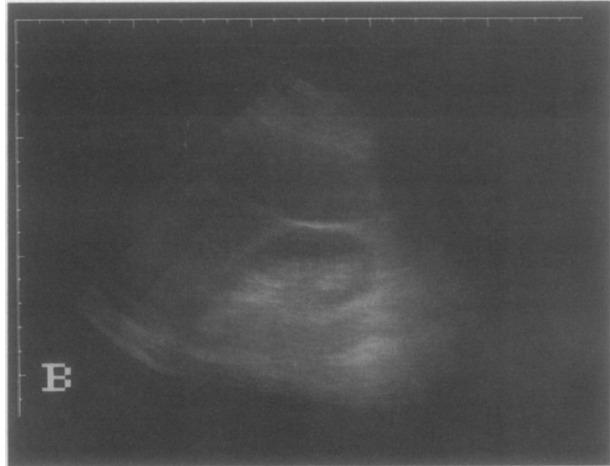
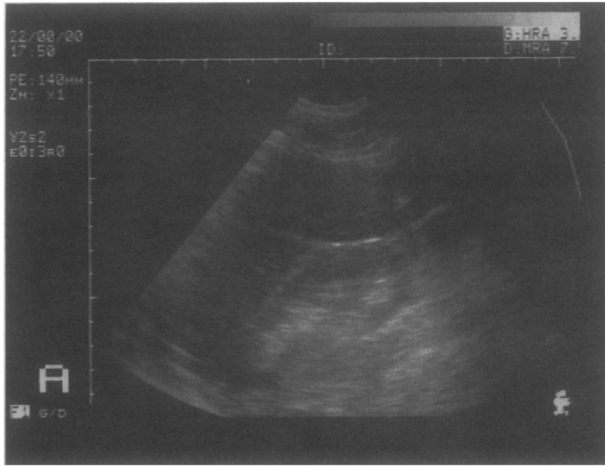


Fig. 8. Speckle reduction on a partial view of the kidney and the liver of a normal subject. (A) One of the 11 images acquired on a same cross-section plane of the kidney and the liver. (B) Speckle reduction after the registration and the average of six of the acquired images.

$$\mu_{u,v}^{k,n}(I,J) = \frac{1}{IJ} \sum_{i=1}^I \sum_{j=1}^J P_{u,v}^{k,n}(i,j) \quad (1)$$

$$\sigma_{u,v}^{k,n}(I,J) = \left[\frac{1}{IJ-1} \sum_{i=1}^I \sum_{j=1}^J (P_{u,v}^{k,n}(i,j) - \mu_{u,v}^{k,n}(I,J))^2 \right]^{1/2} \quad (2)$$

$$\text{SNR}_{u,v}^{k,n}(I,J) = \frac{\mu_{u,v}^{k,n}(I,J)}{\sigma_{u,v}^{k,n}(I,J)} \quad (3)$$

$$k \in [1 \dots C_N^n] \quad n \in [1 \dots N]$$

where $I \times J$ represents the dimensions of the chosen window (I and J are odd numbers); (u,v) indicates the coordinates of the central pixel of the window; (i,j) denotes the coordinates of any pixel in the window; n indicates that the resultant image is the average of n -matched images; k denotes that the resultant image is the k th stemming from the combination of n images chosen among N . $P_{u,v}^{k,n}(i,j)$ is the grey level of the pixel of coordinates (i,j) .

Then, the average value of the SNRs is calculated for the set of resulting images obtained with n original images:

$$\text{SNR}_{u,v}^n(i,j) = \frac{1}{C_N^n} \sum_{k=1}^{C_N^n} \text{SNR}_{u,v}^{k,n}(i,j) \quad n \in [1 \dots N] \quad (4)$$

The average SNR for $n = 1$ image is noted SNRO.

The average SNRs for $n \in [1 \dots N]$ are normalized by SNRO. The normalized average SNR of windows 1 to 4 of Fig. 9a and b is, respectively, represented on the curves Fig. 10-1-4, as a function of n . The standard deviation corresponding to each average SNR is shown equally on these curves.

The windows are chosen in a homogeneous area without artefacts and without specular reflexion. The windows in Fig. 9a have a size of 20×20 pixels and the windows in Fig. 9b have a size of 10×10 pixels. According to the results in Fig. 10, the theory seems to be upheld. In fact, these curves show that the SNR for N -averaged independent images is approximately equal to \sqrt{n} . Moreover, SNRO has the same size order as the value given by Thijssen et al. (1988) ($\cong 4 \times 1.91 = 7.64$), except for window 9A2 (SNRO = 12.037). In this latter case, the talc mixed with agar gel seems to generate specular reflexion and this leads to a higher value of the SNRO.

CONCLUSIONS

A spatial compounding system has been developed to suppress acoustic shadows and to reduce speckle in echographic B-mode images. The spatial localization of images is obtained with an articulated scan arm. The method of reconstruction has been validated on agar gel phantoms. Cross-sectional images of the arm and the thigh of a human subject have been reconstructed without shadows thanks to this method. These images provide information about the geometry of the femur and the humerus, and on the nature of the surrounding soft tissues. This technique could be useful in infant orthopedics to improve the diagnostic capabilities in hip maturational disorders. Spatial com-

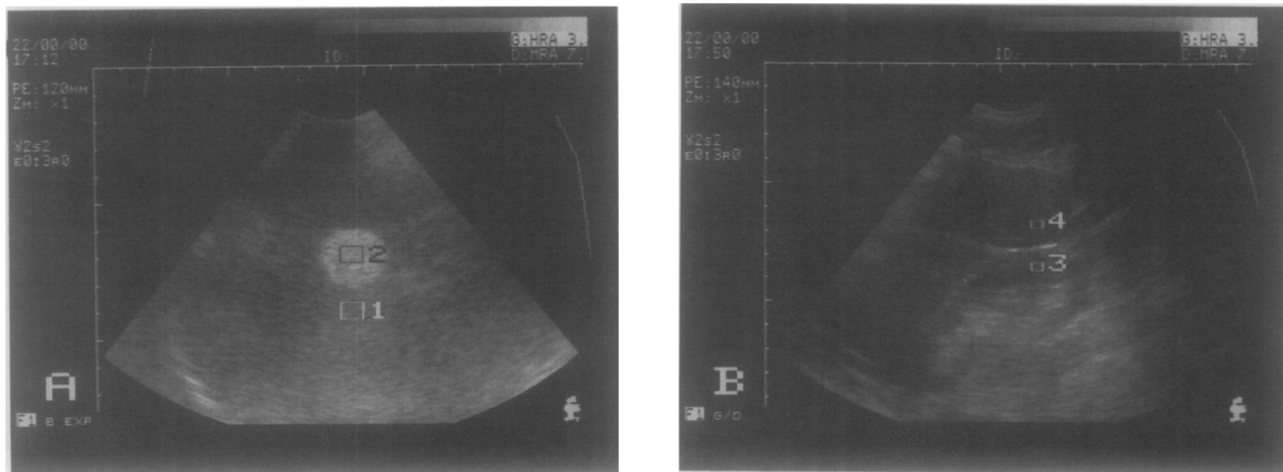


Fig. 9. Localization of the windows in which the SNR is calculated. (A) Agar gel phantom. The window (A1) is representative of a homogeneous area of agar and the window (A2) of talc mixed with agar. (B) A part of the kidney and of the liver of a normal subject. The window (B3) is placed on the cortex of the kidney and the window (B4) on the liver.

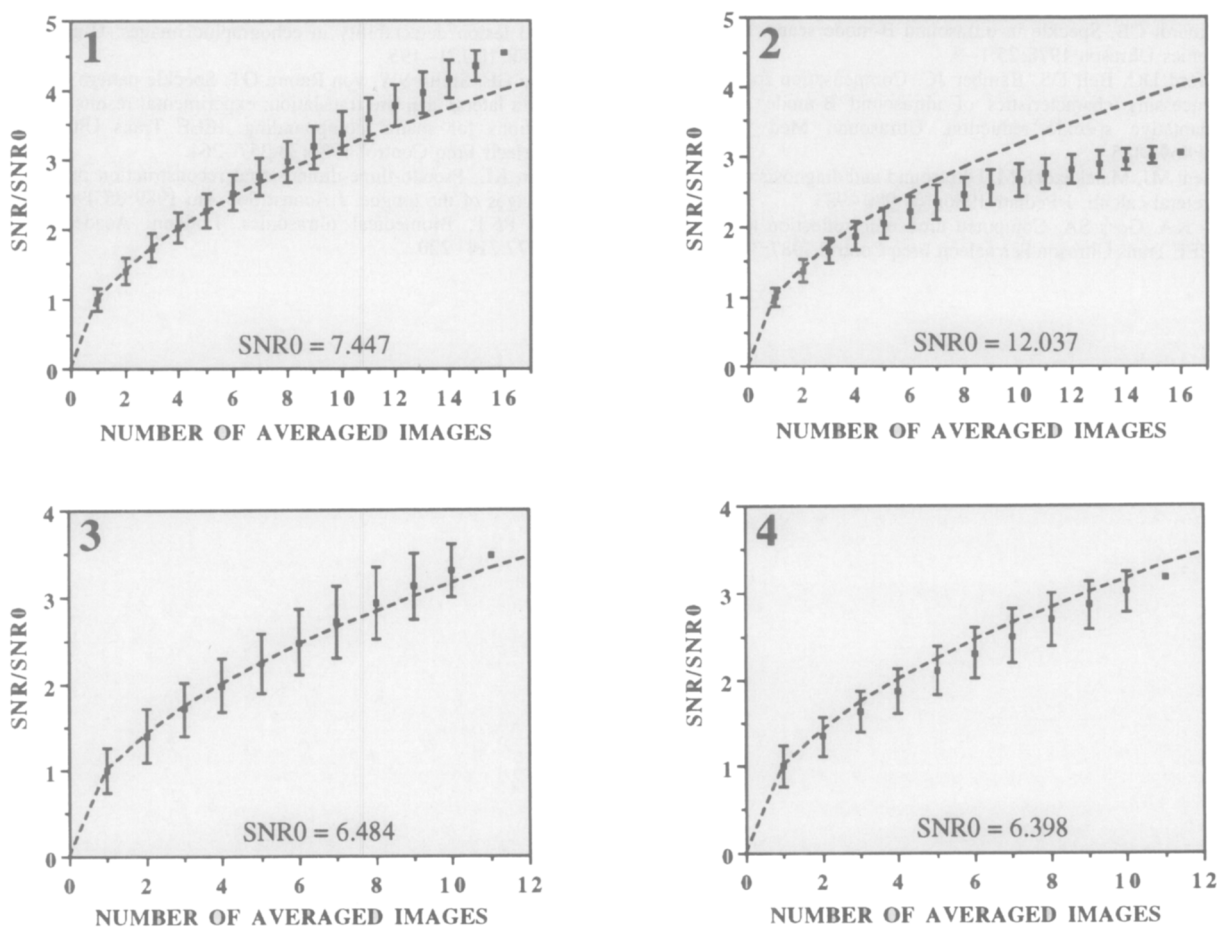


Fig. 10. Normalized average SNR in function of the number of compounded images for different windows. Curves 1–4 correspond to the windows 1, 2, 3 and 4, respectively, of the Fig. 9A and B. The dotted line represents the square root function.

pounding of decorrelated images has shown an obvious reduction of speckle in liver images. The increase of the SNR as a function of the number of registered images seems to uphold the theory by approximately following the square root function.

The use of a scan arm enables the probe to be manipulated using the same conditions as for a usual examination. It represents an inexpensive system for speckle and shadow reduction because every existing B-scan imaging system could be used for this purpose. There are other types of localization systems: electromagnetic (Ganapathy and Kaufman 1992); acoustic (Brinkley et al. 1982; King et al. 1990); or optical (Mills and Fuchs 1990; Watkin 1989). In echographic fields, the latter are mainly used for three-dimensional reconstruction. They suppress the mechanical constraint of the B-scan arm, but they are still onerous and introduce new constraints.

REFERENCES

- Brinkley JF, Muramatsu SK, McCallum WD, Popp RL. In vitro evaluation of an ultrasonic three-dimensional imaging and volume system. *Ultrason Imag* 1982;4:126–139.
- Burckhardt CB. Speckle in ultrasound B-mode scans. *IEEE Trans Sonics Ultrason* 1978;25:1–6.
- Crawford DC, Bell DS, Bamber JC. Compensation for the signal processing characteristics of ultrasound B-mode scanners in adaptative speckle reduction. *Ultrasound Med Biol* 1993; 19:469–485.
- Diament MJ, Malekzadeh M. Ultrasound and diagnosis of renal and ureteral calculi. *J Pediatr* 1986;109:980–983.
- Dines KA, Goss SA. Computed ultrasonic reflection tomography. *IEEE Trans Ultrason Ferroelectr Freq Control* 1987;34:309–318.
- Friedrich M, Hundt E, Maderlechner G. Computerized ultrasound echo tomography of the breast. *Eur J Radiol* 1982;2:78–87.
- Ganapathy U, Kaufman A. 3D acquisition and visualization of ultrasound data. *SPIE Visual Biomed Comput* 1992;1808:535–545.
- Graf R. Fundamentals of sonographic diagnosis of infant hip dysplasia. *J Pediatr Orthop* 1984;4:735–740.
- Greenleaf JF, Bahn RC. Clinical imaging with transmissive ultrasonic computerized tomography. *IEEE Trans Biomed Eng* 1981;28:177–185.
- Hottier F, Collet Billon A. 3D echography: Status and perspective. In: Höhne KH, ed. *3D imaging in medicine*. Berlin: Springer-Verlag, 1990:21–41.
- Jago JR, Whittingham TA. The use of measured acoustic speed distributions in reflection ultrasound CT. *Phys Med Biol* 1992;37:2139–2142.
- King DL, King DL Jr, Yi-Ci Shao M. Three-dimensional spatial registration and interactive display of position and orientation of real-time ultrasound images. *J Ultrasound Med* 1990;9:525–532.
- Mills PH, Fuchs H. 3D ultrasound display using optical tracking. First Conference on Visualization in Biomedical Computing (Atlanta, GA). *IEEE Comput Soc Press* 1990:490–497.
- Nikravesh PE, Skorton DJ, Chandran KB, et al. Computerized three-dimensional finite element reconstruction of the left ventricle from cross-sectional echocardiograms. *Ultrason Imag* 1984; 6:48–59.
- Sehgal CM, Lewallen DG, Nicholson JA, Robb RA, Greenleaf JF. Ultrasound transmission and reflection computerized tomography for imaging bones and adjoining soft tissues. *IEEE Ultrason Symp (Chicago, IL)* 1988;2:849–852.
- Shattuck DP, von Ramm OT. Compound scanning with a phased array. *Ultrason Imag* 1982;4:93–107.
- Thijssen JM, Oosterveld BJ, Wagner RF. Gray level transforms and lesion detectability in echographic images. *Ultrason Imag* 1988;10:171–195.
- Trahey GE, Smith SW, von Ramm OT. Speckle pattern correlation with lateral aperture translation: experimental results and implications for spatial compounding. *IEEE Trans Ultrason Ferroelectr Freq Control* 1986;33:257–264.
- Watkin KL. Pseudo-three-dimensional reconstruction of ultrasonic images of the tongue. *J Acoust Soc Am* 1989;85:496–499.
- Wells PNT. *Biomedical ultrasonics*. London: Academic Press, 1977:214–220.